Unraveling the Pivotal Impacts of Electron-Acceptors on Light Absorption and Carrier Photogeneration in Perylene Dye Sensitized Solar Cells

ARTICLE · AUGUST 2014

DOI: 10.1021/ph5001346

ACS Photonics

Article

pubs.acs.org/journal/apchd5

Unraveling the Pivotal Impacts of Electron-Acceptors on Light Absorption and Carrier Photogeneration in Perylene Dye Sensitized Solar Cells

Min Zhang,[†] Zhaoyang Yao,[†,‡] Cancan Yan,[†,‡] Yanchun Cai,[†] Yameng Ren,[†,‡] Jing Zhang,[†] and Peng Wang*[,†]

[†]State Key Laboratory of Polymer Physics and Chemistry, Changchun Institute of Applied Chemistry, Chinese Academy of Sciences, Changchun, 130022, China

[‡]University of Chinese Academy of Sciences, Beijing, 100049, China

Supporting Information

ABSTRACT: Understanding the ultrafast dynamics of excited state evolution and carrier generation at the complicated titania/dye/electrolyte interface is crucial for the development of narrow energy-gap organic dyes to enhance the performance of dye-sensitized solar cells (DSCs). We herein modulate the energy-levels of *N*-annulated perylene dyes in significant measure by use of benzothiadiazole-benzoic acid (BTBA) and pyridothiadiazole-benzoic acid (PTBA) segments as the electron-acceptors. Based on the model of cold vs hot excited states for electron injection in DSCs, we have perceived from femtosecond transient absorption measurements that a driving force diminution does not necessarily cause a deceleration of electron injection from the hot excited state to titania, suggesting a crucial role of electron coupling on interfacial charge transfer kinetics. Moreover, the electron-accetpor variation from BTBA to PTBA brings forth a fast relaxation of the hot excited state as well as a rapid deactivation of the cold excited state and a sluggish electron injection from the cold excited state to titania. These adverse multichannel kinetics jointly result in a remarkable diminishment of overall electron injection yield and, thus, lower external quantum efficiency of cell with the PTBA dye. Our studies have highlighted the importance of considering the excited state topology on the future design of low energy-gap photovoltaic materials.

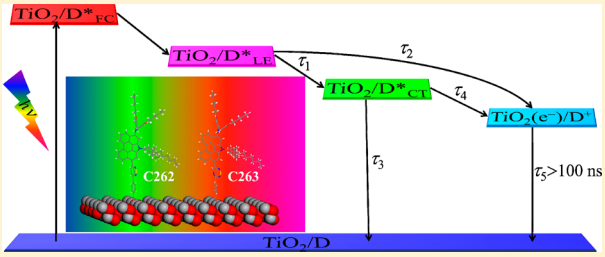

KEYWORDS: *solar cell, organic dye, light absorption, excited state, charge transfer*

Since the pioneering work by O'Regan and Grätzel in 1991,[1] the dye-sensitized solar cell (DSC) has attracted considerable research interest as an eco-friendly and low-cost technology for the conversion of solar energy to clean electricity. In this photovoltaic device, a sensitizing dye plays a momentous role in determining the cell efficiency by impacting light absorption, carrier generation, and charge recombination.[2−13] To date the best performed sensitizers are some ruthenium polypyridine and zinc porphyrin complexes in terms of cell stability and efficiency.[14−18] On the other aspect, enormous research passions have also been devoted to the synthesis of a large number of metal-free organic dyes.[4,6,8,9,11]

Credited with excellent photophysical properties such as large molar absorption coefficients and high fluorescence yields, the perylene derivatives possessing coplanar electronic skeleton have been widely applied in various optical and electrical devices.[19,20] However, perylene as a building block of sensitizers for DSCs has only attracted moderate interest[21−28] since the earlier work by Ferrere et al.,[29] and so far the perylene dyes, have not attained very excellent performance. Very recently, we have synthesized a metal-free perylene dye (**C261**, Figure 1), featuring a bisarylamino functionalized *N*-annulated perylene electron-releasing segment and a cyanoacrylic acid (CA) electron-withdrawing unit, which displays an impressive power conversion efficiency (PCE) of 8.8% at an irradiance of the air mass 1.5 global (AM1.5G) sunlight.[30]

Keeping in mind our success on the employment of benzothiadiazole-benzoic acid (BTBA) as the electron-acceptor for a low energy-gap organic dye to achieve the so far highest efficiency of organic dye-sensitized solar cells,[31] and the important observation that the acceptor variation from CA to BTBA for triphenylamine-cyclopentadithiophene dyes brings forth red-shifted absorptions for both dye solutions and dye-grafted titania films (see Supporting Information for a detailed discussion), we have aimed to replace the CA acceptor of the **C261** dye with BTBA to construct a new dye (**C262**, Figure 1). Our preliminary theoretical calculations have shown that there is a large torsion angle between the perylene and benzothiadiazole (BT) units in **C262**, leading to an evidently blue-shifted absorption peak compared to **C261** (see Supporting Information for a detailed discussion). Thereby,

Received: April 23, 2014
Published: July 15, 2014

   dx.doi.org/10.1021/ph5001346 | *ACS Photonics* 2014, 1, 710−717

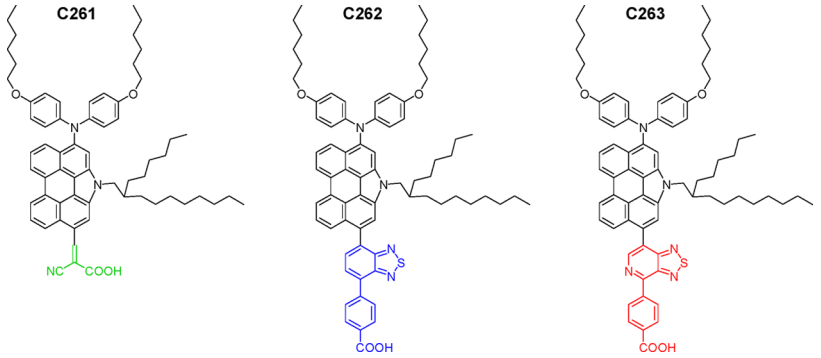

Figure 1. Molecular structures of the bisarylamino functionalized *N*-annulated perylene dyes **C262** and **C263**, characteristic of BTBA (blue) and PTBA (red) electron-acceptors. The previously reported **C261** dye with the CA (green) electron-acceptor is also included for comparison.

we have further considered the more electron-withdrawing pyridothiadiazole (PT) unit to reduce the energy-gap and design the **C263** dye (Figure 1). Based upon a tris(2,2′-bipyridine)cobalt (Co-bpy) electrolyte, in this contribution we will employ photophysical and electrical measurements in conjunction with theoretical tools to perform a systematic comparison on the impacts of BTBA and pyridothiadiazole-benzoic acid (PTBA) on energy level, light absorption, and carrier photogeneration, which underpin the phenomenal photovoltaic performance of DSCs.

RESULTS AND DISCUSSION

We first measured cyclic voltammograms (Figure 2) of **C262** and **C263** dissolved in tetrahydrofuran (THF) and derived the highest occupied molecular orbital (HOMO) and the lowest unoccupied molecular orbital (LUMO) energy levels as listed in Table 1. The more electron-deficient block of PTBA endows the **C263** dye with an obviously lower LUMO (−3.57 eV vs vacuum) and a comparable HOMO (−4.89 eV), with respect to **C262** characteristic of the BTBA segment (LUMO: −3.25 eV; HOMO: −4.87 eV). This results in a smaller energy-gap for **C263** in comparison with **C262**. As compiled in Table 1, the relative tendencies of experimentally measured energy levels can be well mimicked by our density functional theory (DFT) calculations at the B3LYP/6-311G(d,p) level.

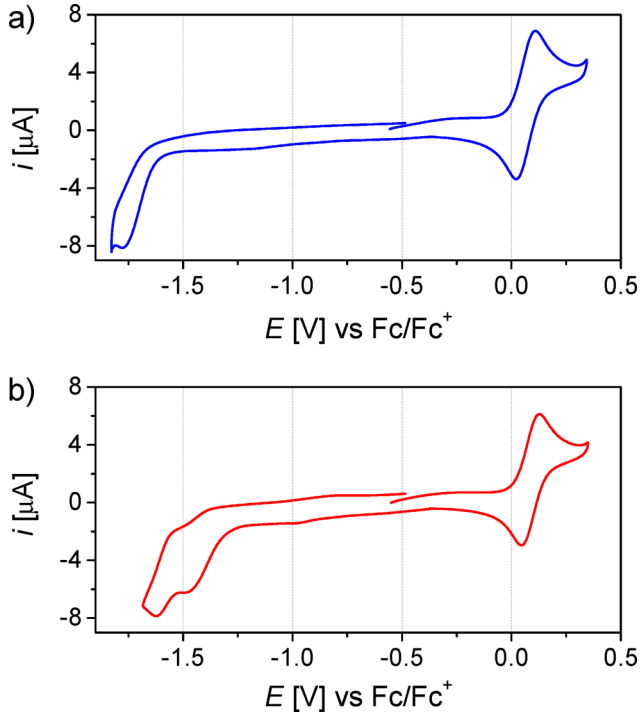

Figure 2. Cyclic voltammograms of (a) **C262** and (b) **C263** in THF with 0.1 M EMITFSI as the supporting electrolyte. Working electrode: glassy carbon; scan rate: 5 mV s^{-1}.

The electronic absorption spectra of **C262** and **C263** dissolved in THF were also recorded to preliminarily evaluate the influence of electron-acceptor on the solar photon harnessing power. As depicted in Figure 3b, the **C263** dye featuring the PTBA acceptor displays overlapped absorption bands in the visible region, which can be separated into three bands via multipeak Gaussian fitting, two of which are centered at 472 and 540 nm, respectively (Table 1). The latter peak is red-shifted by 37 nm with respect to that of 503 nm (Figure 3a) for **C262** with BTBA as the electron-acceptor. To gain insight into the acceptor dependent absorption spectra, we further resorted to the time dependent density functional theory (TDDFT) calculation to mimic the absorptions of **C262** and **C263**. As shown in Figure 3, there is a good consistence between the experimental and theoretical absorption bands. The calculated absorption wavelengths (λ_{abs}^{calc}) and transition assignments are also compiled in Table 1. In general, the absorption spectra of both **C262** and **C263** in the visible region are originated from the $S_0 \rightarrow S_1$ and $S_0 \rightarrow S_2$ transitions. For both dyes, the $S_0 \rightarrow S_2$ transition to LUMO+1 is related to HOMO and the $S_0 \rightarrow S_1$ transition to LUMO is mainly involved with HOMO and HOMO−1. Further analyses on the corresponding molecular orbital topologies (Figure S4) disclose that the low-energy absorption band ($S_0 \rightarrow S_1$) can be assigned to the intramolecular charge transfer transitions from the bisarylamino functionalized *N*-annulated perylene electron-donating unit to the BTBA or PTBA electron-withdrawing segment.

The remarkable energy-gap shrinkage endowed by transforming the electron-acceptor of a perylene dye from BTBA to PTBA can be more clearly perceived from Figure 4a, in which light harvesting efficiency (ϕ_{lh}) of dye-grafted mesoporous titania films was plotted as a function of wavelength. Furthermore, by recording the small but reliable light-absorption change of a dyeing solution at a certain volume, we could roughly estimate the loading amount (c_m) of dye molecules on titania. It is found that there is an increased c_m of 2.22×10^{-8} mol cm^{-2} μm^{-1} for **C263**, in contrast to that of 1.97×10^{-8} mol cm^{-2} μm^{-1} for **C262**. To gain insights on the origin of different dye load amounts, we first took a look at

dx.doi.org/10.1021/ph5001346 | ACS Photonics 2014, 1, 710−717

Table 1. Measured and Calculated Energy Levels, Energy-Gaps, and Electronic Absorption Properties of C262 and C263

dye	E_H[a] (eV)	E_L[a] (eV)	E_{H-1}[b] (eV)	E_H[b] (eV)	E_L[b] (eV)	E_{L+1}[b] (eV)	$\Delta E_{H/L}$[b] (eV)	$\Delta E_{H-1/L}$[b] (eV)	$\Delta E_{H/L+1}$[b] (eV)	λ_{abs}^{meas}[c] (nm)	λ_{abs}^{calc}[d] (nm)	transition assignment[d]
C262	−4.87	−3.25	−5.48	−4.84	−2.75	−2.07	2.09	2.73	2.76	465	436	H → L + 1 (95%)
										503	508	H → L (88%) H − 1 → L (8%)
C263	−4.89	−3.57	−5.51	−4.86	−3.12	−2.12	1.74	2.39	2.74	472	442	H → L + 1 (100%)
										540	578	H → L (92%) H − 1→L (8%)

[a]Measured frontier orbital energies with respect to vacuum were calculated via $E = -4.88 - eE_{onset}$, where E_{onset} is the onset potential (Figure 2) of oxidation and reduction of the ground state of a dye measured with cyclic voltammetry. H and L represent HOMO and LUMO, respectively. [b]Frontier orbital energies with respect to vacuum were calculated at the B3LYP/6-311G(d,p) level for a dye in THF. [c]λ_{abs}^{meas} was measured for a dye in THF and the values were obtained via multipeak Gaussian fitting, as presented in Figure 3. [d]λ_{abs}^{calc}, oscillator strength (f), and corresponding transition assignments were derived from the TDDFT calculation at the MPW1K/6-311G(d,p) level for a dye in THF.

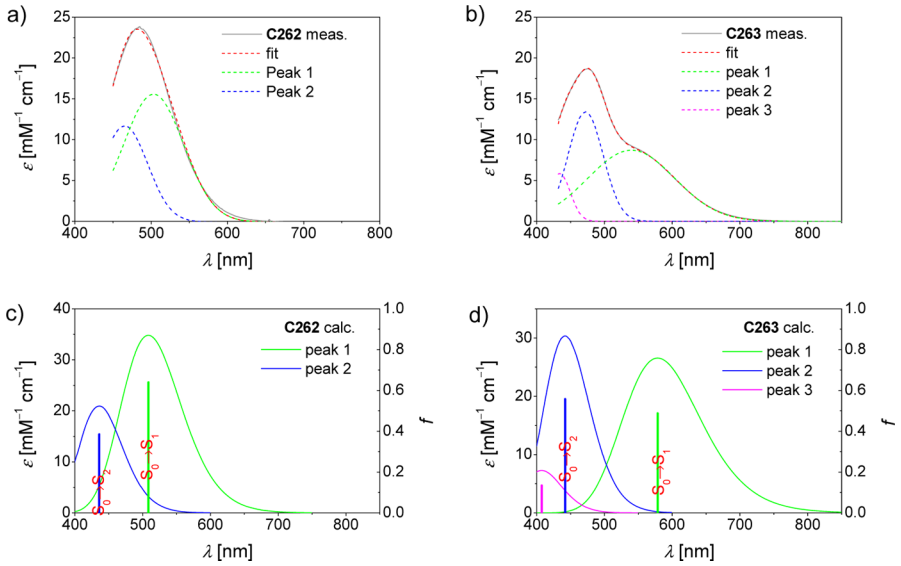

Figure 3. Measured molar absorption coefficients (ε) plotted as a function of wavelength (λ) for the THF solutions of (a) **C262** and (b) **C263**. As shown in panels a and b, multipeak Gaussian fittings nicely reproduce the measured electronic absorption spectra and distinctly afford multiple absorption bands with clear peaks in the visible light region. (c, d) Simulated electronic absorption bands based upon TDDFT calculations on excitation energies shown by the x-coordinates of vertical lines and oscillator strengths (f) by using a Gaussian function with a fixed half-bandwidth of 2000 cm^{-1}. The two main bands originate from the $S_0 \rightarrow S_1$ and $S_0 \rightarrow S_2$ transitions, respectively.

their molecular geometries (Figure S2) and identified smaller torsion angles between adjacent aromatic segments for **C263**. Moreover, the **C263** dye presents a larger dipole moment of 9.7 D in comparison with that of 6.9 D for **C262**. These two points could jointly contribute to a stronger intermolecular $\pi-\pi$ stacking in the self-assembled dye layer on titania. This scenario is in general accord with our previous finding on the possible influence of molecular dipole moment on dye packing.[31] The variation of dye binding strength was not considered here since we did not probe higher electron densities on the two oxygen atoms, belonging to the carboxylic acid anchoring group of **C263**. It is well documented from theoretical calculations that the cyanoacrylic acid anchoring group has an even stronger binding on the titania surface than the malonic acid anchoring group,[32] and consistent conclusions can also be drawn from our DFT calculations in terms of the electron densities on the oxygen atoms of perylene dyes **C261**, **C262**, and **C263**. However, the perylene dye **C261** featuring a cyanoacrylic acid acceptor in our previous paper[30] does not feature a much higher c_m (1.92×10^{-8} mol cm^{-2} μm^{-1}) than **C262** and **C263**, under the same experimental conditions, implying the necessity of a deeper understanding on this complicated topic in the future studies. It may be deduced that the solvation associated adsorption−desorption equilibrium plays a key role in the herein observed dye loading amounts.

The **C262** and **C263** grafted bilayer titania films were combined with a Co-bpy electrolyte to fabricate DSCs. The details for cell fabrication are described in the Experimental Section. As depicted in Figure 4b, a perceptible bathochromic photocurrent onset wavelength can be noted upon the substitution of BTBA with PTBA, in good accordance with the preceding electronic absorption data (Figure 4a). However, the **C263** cell exhibits a remarkably lower external quantum efficiency (EQE) summit of only 45%, compared to that of 81% for **C262**, albeit its saturated absorption in a broad visible and near-IR spectral region (Figure 4a).

We further measured femtosecond transient absorption (fs-TA) spectra (Figure 5a,b) to directly survey the photoinduced electron injection dynamics and electron injection yields of the dye-grafted mesoporous titania films immersed in the Co-bpy electrolyte.[33,34] The severe spectroscopic superposition of the ground state, excited state, and charge-separated state for the herein tested samples has actually excluded the possibility of probing the electron injection dynamics by monitoring the signals at a selected wavelength in this spectral region (Figures S5 and S6). By use of the kinetic model of cold versus hot excited states for electron injection in DSCs (Scheme 1)

dx.doi.org/10.1021/ph5001346 | ACS Photonics 2014, 1, 710−717

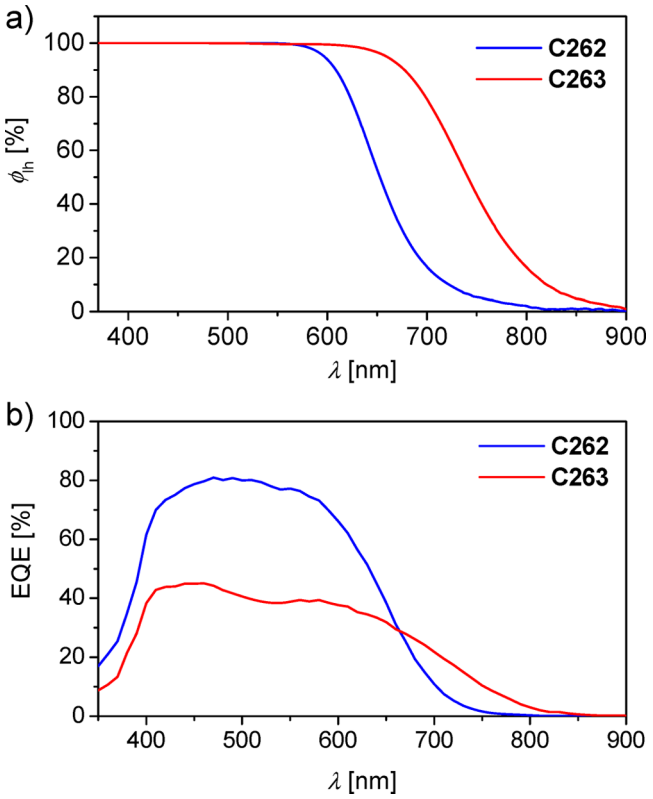

Figure 4. (a) Plots of light harvesting efficiencies (ϕ_{lh}) as a function of wavelength (λ) for 10-μm-thick, dye-grafted mesoporous titania films immersed in a Co-bpy electrolyte for DSC fabrication. (b) Plots of external quantum efficiencies (EQE) as a function of wavelength (λ) for cells made with dye-grafted bilayer (4.3 + 5.0 μm thick) titania films and a Co-bpy electrolyte.

proposed in our previous work,[30,35] we performed target analysis[36−38] of the recorded fs-TA data and identified four key species in the kinetic evolution, including the Franck−Condon excited state (D^*_{FC}), the locally excited state (D^*_{LE}), the intramolecular charge-transfer state (D^*_{CT}), and the charge-separated state [$TiO_2(e^-)/D^+$] as represented in the species-associated difference spectra (SADS) of Figure 5c,d. D^*_{CT} is considered as the cold excited state with respect to the hot excited states D^*_{FC} and D^*_{LE}. Note that we have not distinguished the stimulated emission (SE) from the excited state absorption (ESA). In addition, we have fixed the time constant of generating D^*_{LE} from D^*_{FC} via relaxation of the Franck−Condon vibrational wave packet as ∼150 fs in view of the limited time response of our measurement system. The validity of this assumption has been somehow supported by the fact that the whole TA spectra do not feature any excitation wavelength dependence. By use of the extracted time constants presented in Scheme 1, both kinetic traces at a series of wavelengths (Figures S5 and S6) and difference spectra (Figures S7 and S8) at a set of time delays can be reproduced very nicely. The kinetic traces of some key components of D^*_{FC}, D^*_{LE}, D^*_{CT}, and $TiO_2(e^-)/D^+$ are presented in Figure 5e,f.

The time constants (τ_1) for the conversion from D^*_{LE} to D^*_{CT} possibly via torsional relaxation are 5.3 ps for **C262** and 1.2 ps for **C263**. This could be roughly understood with a view on a smaller torsion angle between BA and PT units (Figure S2), which is consistent with our previous comparison on other two donor−π-linker−acceptor (D-π-A) dyes with the respective twisted and coplanar π-linkers.[35] The slower exothermic excited-state relaxation from the D^*_{LE} state to D^*_{CT} observed for the **C262** dye ensures a higher branching ratio of electron injection from D^*_{LE}, even if the rate of electron injection from D^*_{LE} for **C262** is not as fast as **C263**. Considering that the dye transformation from **C262** to **C263** just brings forth a negligible downward shift of the titania conduction-band edge (∼15 meV, see the details in the following discussion), the remarkably lower LUMO energy level (over 300 meV) of **C263** will results in a smaller driving force of electron injection from D^*_{LE} with respect to **C262**. Thereby, the more rapid electron injection from D^*_{LE} for **C263** could be ascribed to a stronger electron coupling of D^*_{LE} and titania, which could originate from a smaller torsion angle between the PT and BA units.[39] Moreover, with respect to **C262**, the electron injection from D^*_{CT} for **C263** is more dilatory, which along with a shorter time constant of deactivation from its D^*_{CT} state to ground state (see Scheme 1 for details) leads to a very low branching ratio of electron injection from D^*_{CT}. Regarding the electron injection from D^*_{CT}, the tardy electron injection for **C263** may be dominated by the smaller driving force. In addition, the significantly narrower energy gap is responsible for the accelerated radiationless deactivation from the D^*_{CT} state to the ground state for **C263**, which could become increasingly favorable (at an exponential rate) with a reduced energy-gap.[40] The averaged time constants ($\tilde{\tau}_{ei}$) for the two-exponential generation of D^+ from D^*_{LE} and D^*_{CT} are 14.3 ps for **C262** and 21.9 ps for **C263**. Furthermore, on the basis of extracted time constants, we can calculate the respective electron injection efficiencies (ϕ_{ei}) to be 87% and 52% for cells made from **C262** and **C263** in terms of equation $\phi_{ei} = \tau_1/(\tau_1 + \tau_2) + [\tau_2/(\tau_1 + \tau_2)] \times [\tau_3/(\tau_3 + \tau_4)]$, accounting for the aforementioned lower EQE summit of **C263** with respect to **C262**.

We further recorded the photocurrent density−voltage (j−V) characteristics at an irradiance of 100 mW cm^{-2}, simulated AM1.5 sunlight (Figure 6a) of cells made from **C262** and **C263** to evaluate the influence of electron-acceptor on photovoltaic parameters, and the detailed parameters are listed in Table 2. The short-circuit photocurrent density (j_{sc}), open-circuit photovoltage (V_{oc}), and fill factor (FF) of the cell with **C262** are 12.63 mA cm^{-2}, 788 mV, and 0.730, respectively, generating a PCE of 7.3%. Nevertheless, in good agreement with the photocurrent densities (j_{sc}^{EQE}, Table 2) predicted by integrating the EQEs over the whole AM1.5G spectrum, the cell with **C263** featuring a smaller energy-gap displays a lower j_{sc} of 8.83 mA cm^{-2}. Moreover, the **C263** cell exhibits an over 40 mV reduced V_{oc} of 742 mV, affording a markedly decreased PCE of 5.0%. For a DSC at the short-circuit condition of a considerable low electron density in mesoporous titania film, the measured j_{sc} is roughly proportional to the carrier photogeneration flux, which motivates us to further measure j−V curves under various light irradiances and plot V_{oc} versus j_{sc} (Figure 6b) and compare the acceptor correlated V_{oc} variation at a given j_{sc}. It is noted that the **C262** cell exhibits an obviously higher V_{oc} compared to **C263** at a certain j_{sc}.

For DSCs with a fixed redox electrolyte, it is well documented that the value of V_{oc} under light is intimately related to the electron quasi-Fermi-levels ($E_{F,n}$) of titania, which is jointly determined by the conduction band edge (E_c) of titania and the density of electrons stored in titania.[41,42] Moreover, at a certain flux of carrier photogeneration, the density of electrons in titania is governed by the rate of recombination between photoinjected electrons with holes in the electrolyte and/or the oxidized dye molecules. Therefore,

dx.doi.org/10.1021/ph5001346 | ACS Photonics 2014, 1, 710−717

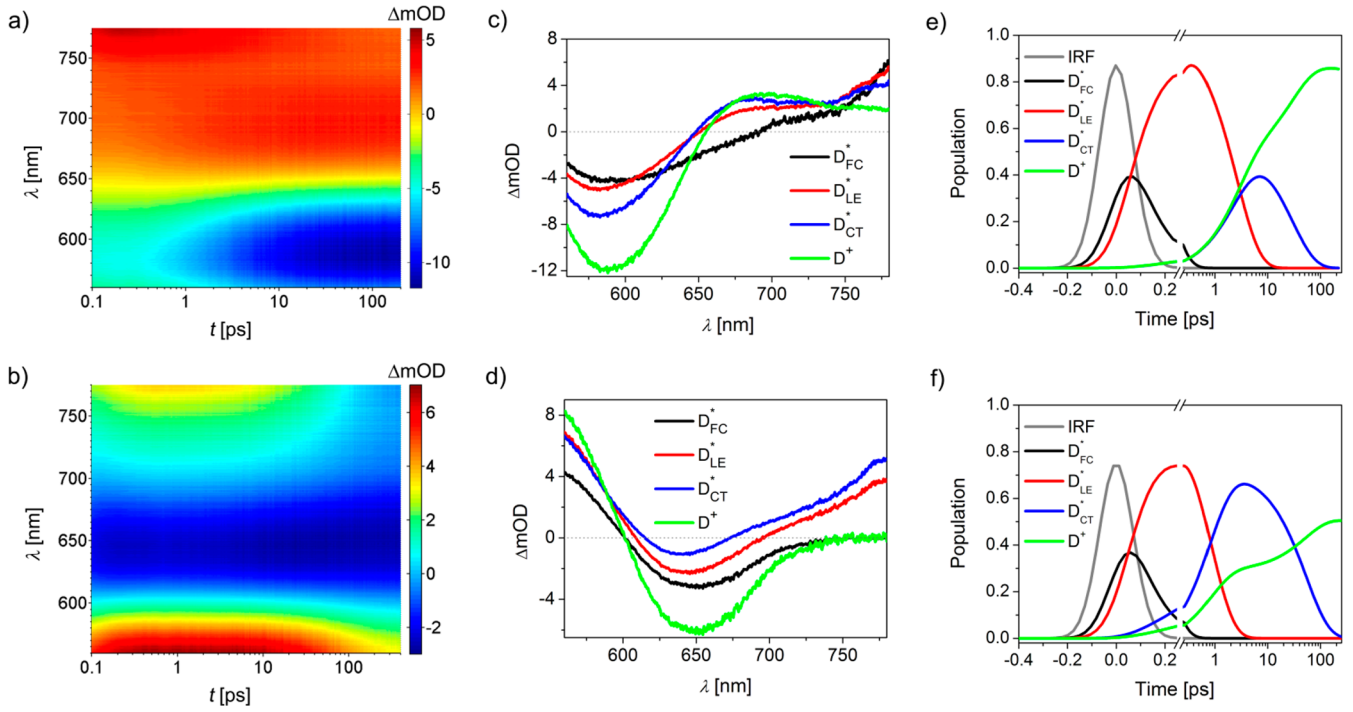

Figure 5. (a, b) fs-TA spectra of 2.1 μm thick, mesoporous titania films grafted with **C262** (panel a) and **C263** (panel b), which are also in contact with a Co-bpy electrolyte. The pulse fluence of pump light at 530 nm is 7 uJ cm^{-2}. (c, d) Species-associated difference spectra of D^*_{FC}, D^*_{LE}, D^*_{CT}, and D^+ for the **C262** (panel c) and **C263** (panel d) samples, which are generated via target analysis of the spectra in panels a and b. Note that we did not separate the small contribution of the transition of photoinjected electrons in titania from the nominal spectra of D^+. (e, f) Kinetic traces generated by target analysis, for D^*_{FC} (black), D^*_{LE} (red), D^*_{CT} (blue), and D^+ (green) of the **C262** (panel e) and **C263** (panel f) samples. The gray lines in panels e and f represent the instrument response functions.

Scheme 1. Model of Cold vs Hot Excited State for Electron Injection Used in the Target Analysis of fs-TA Spectra of C262 (left) and C263 (right) Grafted Titania Films[a]

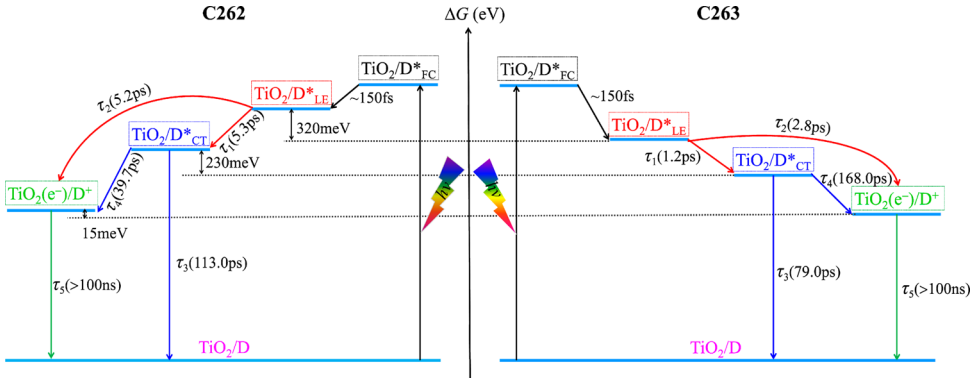

[a]Time constants derived from target analysis of fs-TA spectra are also included. The energy difference of TiO_2/D^*_{LE} is derived from the LUMO measurements of these two dyes. The energy difference of TiO_2/D^*_{CT} is derived from the Stokes shift measurements of these two dyes in Figure S9. The titania conduction band edge difference is derived from the charge extraction measurements.

we further carried out the charge extraction (CE) and transient photovoltage decay (TPD) measurements to examine the origins of aforesaid acceptor related V_{oc} difference by analyzing the interfacial energetics and kinetics.[43,44] As depicted in Figure 7a, the sensitizer alteration from **C262** to **C263** brings forth a 15 mV downward shift of the E_c of titania. This variation may originate from a lower dye load amount for **C262** with respect to **C263**, which allows more *tert*-butylpyridine (TBP) to adsorb on the surface of titania in the **C262** cell.[45] Moreover, the dye change from **C262** to **C263** leads to a perceivably smaller time constant (τ_e) at a given Q, as illustrated in Figure 7b. The relatively lower E_c and faster interfacial recombination in the **C263** cell jointly explain the aforementioned lower V_{oc} at a given j_{sc} compared to **C262**. As shown in Figure S10, impedance spectroscopy (IS) measurements[41] have shown that these two cells have very similar electron diffusion lengths at a given density of state (DOS), suggesting the electron collection efficiency is not likely to exert a significant influence on the EQE summit variation.

CONCLUSIONS

In summary, we have employed benzothiadiazole-benzoic acid and pyridothiadiazole-benzoic acid as the electron-acceptors to tune the energy-gaps of bisarylamino functionalized *N*-

dx.doi.org/10.1021/ph5001346 | ACS Photonics 2014, 1, 710−717

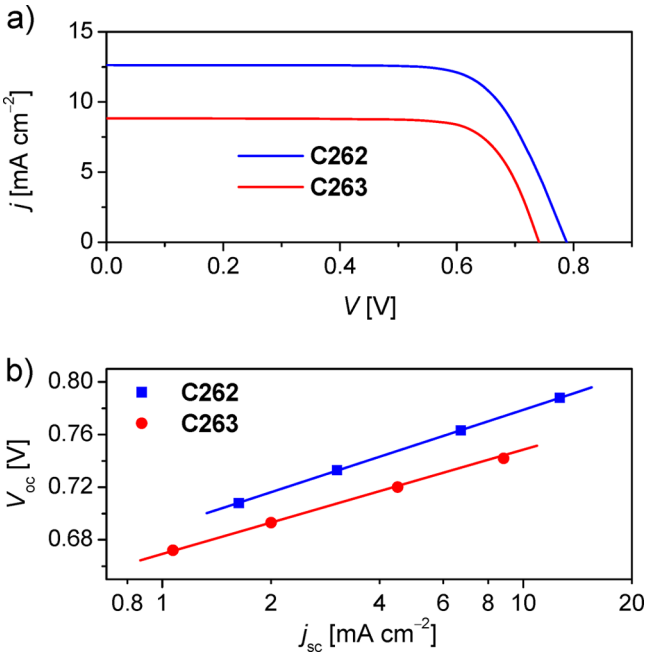

Figure 6. (a) Current−voltage (j−V) characteristics measured at an irradiance of 100 mW cm^{-2}, simulated AM1.5 sunlight. (b) Plots of open-circuit photovoltage (V_{oc}) against short-circuit photocurrent (j_{sc}). An antireflection film was adhered to the testing cells during measurements. The aperture area of the employed metal mask is 0.160 cm^{-2}.

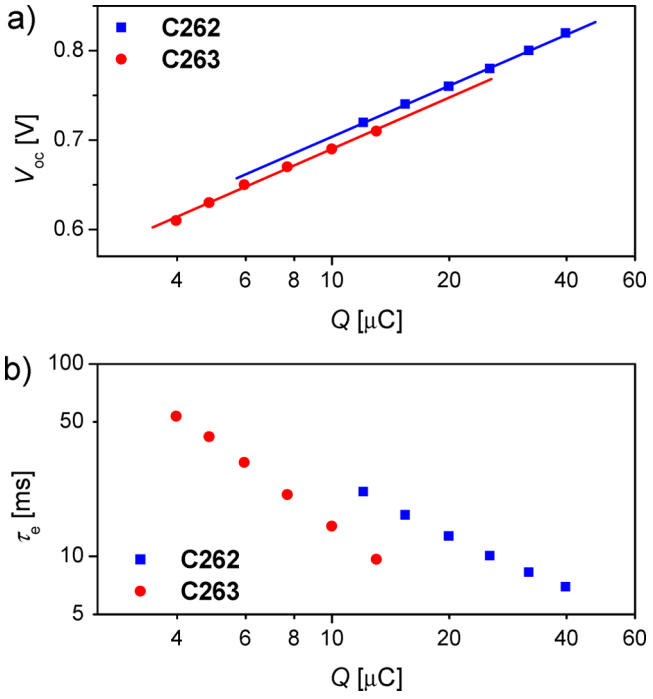

Figure 7. (a) Relationship of charge stored in the dye-grafted titania film (Q) and open-circuit photovoltage (V_{oc}). The line is just drawn as a guide to the eye. (b) Plots of lifetime of photoinjected electrons in titania (τ_e) as a function of charge.

annulated perylene dyes. Both theoretical calculations and experimental measurements have proved that the replacement of benzothiadiazole with a more electron-deficient pyridothiadiazole can lower the LUMO energy level of a perylene dye to reduce the energy-gap for an enhanced light absorption. It is valuable to note that the driving force reduction accompanied by a lower LUMO does not necessarily cause a decreased rate of electron injection from the hot excited state. The electron injection kinetics from the hot excited state perhaps has been dominated by a strong electron coupling of the high-energy excited state and titania, owing to a smaller torsion angle between the pyridothiadiazole and benzoic acid units. However, the quick relaxation of the hot excited state, the fast deactivation of the cold excited state to the ground state, and the sluggish electron injection of the cold excited state jointly give rise to a remarkable reduction of the overall electron injection yield for the pyridothiadiazole attached perylene dye and thus a lower external quantum efficiency. Our findings presented here could give some important implications on the further rational design of narrow energy-gap organic dyes.

EXPERIMENTAL SECTION

Materials. THF, ethanol, and chloroform were distilled before use. Lithium bis(trifluoromethanesulfonyl)imide (LiTFSI), 1-ethyl-3-methylimidazolium bis(trifluoromethanesulfonyl)imide (EMITFSI), and TBP were purchased from Sigma-Aldrich. The synthetic details of **C262** and **C263** are described in the Supporting Information.

Theoretical Calculations. The ground state geometries of dye molecules were optimized with the DFT method by employing the popular three-parameter B3LYP function.[46] During structure optimization the frequency analysis was also performed to rule out the presence of imaginary frequency. For the calculations on vertical excitation energies and oscillator strengths, we used the TDDFT method by picking the hybrid functional MPW1K,[47] which has been considered as a suitable selection for donor−acceptor organic dye.[48] In all the calculations, the 6-311G (d, p) basis set was selected and the conductor-like polarized continuum model (C-PCM)[49] method was used to simulate the solvent effect. All calculations were carried out with the Gaussian 09 program package.

DSC Fabrication and Characterization. A 4.3 + 5.0 μm thick, bilayer titania film deposited via screen-printing on a precleaned fluorine-doped tin oxide (FTO) conducting glass

Table 2. Averaged Photovoltaic Parameters of Four Cells Measured at an Irradiance of 100 mW cm^{-2} Simulated AM1.5 Sunlight[a]

dye	j_{sc}^{EQE} (mA cm^{-2})	j_{sc} (mA cm^{-2})	V_{oc} (mV)	FF	PCE (%)
C262	12.81 ± 0.17	12.63 ± 0.15	788 ± 3	0.735 ± 0.005	7.3 ± 0.2
C263	8.67 ± 0.15	8.83 ± 0.13	742 ± 4	0.768 ± 0.006	5.0 ± 0.2

[a] j_{sc}^{EQE} is derived via wavelength integration of the product of the standard AM1.5 emission spectrum (ASTM G173−03) and the EQEs measured at the short-circuit. The validness of measured photovoltaic parameters is evaluated by comparing the calculated j_{sc}^{EQE} with the experimentally measured j_{sc}.

dx.doi.org/10.1021/ph5001346 | ACS Photonics 2014, 1, 710−717

(Nippon Sheet Glass, Solar, 4 mm thick) was used as the negative electrode of DSCs presented in this paper. A translucent layer of 25 nm sized titania particles was first printed on a FTO glass and further coated by a light-scattering layer of 350−450 nm sized titania particles (WER4-O, Dyesol). The preparation procedures of titania nanocrystals, screen-printing pastes, and nanostructured titania films were very similar to those described in a previous paper.[50] A circular titania electrode (~0.28 cm^2) was dye-grafted by dipping it into a 150 μM dye solution in the binary solvent mixed with chloroform and ethanol at a volume ratio of 1/9 for 10 h. The dye-grafted titania electrode was assembled with a gold-coated FTO electrode with a 25 μm thick Surlyn ring to produce a thin-layer electrochemical cell by heating. The Co-bpy electrolyte is composed of 0.25 M tris(2,2′-bipyridine)cobalt-(II) di[bis(trifluoromethanesulfonyl)imide], 0.05 M tris(2,2′-bipyridine)cobalt(III) tris[bis(trifluoromethanesulfonyl)imide], 0.5 M TBP, and 0.1 M LiTFSI in acetonitrile. Details of EQE, $j-V$, CE, TPD, and IS measurements have been detailed in our previous publications.[51,52]

UV−Vis and Voltammetric Measurements. Steady-state electronic absorption measurements were carried out with an Agilent G1103A spectrometer. Cyclic voltammograms of the THF solutions of dyes were recorded on a CHI660C electrochemical workstation in combination with a three-electrode electrochemical cell consisting of a platinum counter electrode, a silver wire quasi-reference electrode, and a glassy carbon working electrode. All the potentials were reported against the ferrocene/ferrocenium (Fc/Fc^+) reference. The frontier orbital energies with respect to vacuum were estimated via measuring the onset potentials (E_{onset}) of oxidation and reduction of the ground state of a dye via the equation $E = -4.88 - eE_{onset}$.

fs-TA Measurements. A mode-locked Ti:sapphire laser (Tsunami, Spectra Physics) pumped by a Nd:YVO4 laser (Millennia Pro s-Series, Spectra Physics) was employed as the source of a regenerative amplifier (RGA, Spitfire, Spectra Physics) to generate 3.7 mJ, 130 fs pulses at 800 nm. The fs pulses were split into two parts at a ratio of 9/1 with a beam splitter. The large proportion was delivered to an optical parametric amplifier (TOPAS-C, Light Conversion) to produce pump pulses. A white light continuum generated by focusing the minor portion of the output of RGA on a sapphire was split into two equal beams as the probe and reference lights. The probe and reference lights were focused on two optical fibers integrated with monochromators and detected by two multichannel optical sensors (1024 elements, MS 2022i, CDP Corp.). The polarization between pump and probe beams on a rotating sample was set at the magic angle. The processed signal was displayed with the ExciPRO software (CDP Corp.). The raw data were analyzed by using the Glotaran software.[53]

■ ASSOCIATED CONTENT

Supporting Information

Analyses on electron-acceptor dependent energy levels and absorption spectra: CA vs BTBA; The synthetic details of **C262** and **C263**; Optimized geometries and additional spectroscopic data. This material is available free of charge via the Internet at http://pubs.acs.org.

■ AUTHOR INFORMATION

Corresponding Author

*E-mail: peng.wang@ciac.ac.cn. Tel.: 0086-431-85262952.

Notes

The authors declare no competing financial interest.

■ ACKNOWLEDGMENTS

Acknowledgements are made to the National 973 Program (2011CBA00702), the National 863 Program (No. 2011AA050521), and the National Science Foundation of China (Nos. 51103146, 51125015, and 91233206) for financial support.

■ REFERENCES

(1) O'Regan, B.; Grätzel, M. A low-cost, high-efficiency solar cell based on dye-sensitized colloidal TiO_2 films. *Nature* **1991**, *353*, 737−740.
(2) Robertson, N. Optimizing dyes for dye-sensitized solar cells. *Angew. Chem., Int. Ed.* **2006**, *45*, 2338−2345.
(3) Imahori, H.; Umeyama, T.; Ito, S. Large π-aromatic molecules as potential sensitizers for highly efficient dye-sensitized solar cells. *Acc. Chem. Res.* **2009**, *42*, 1809−1818.
(4) Mishra, A.; Fischer, M. K. R.; Bäuerle, P. Metal-free organic dyes for dye-sensitized solar cells: from structure: property relationships to design rules. *Angew. Chem., Int. Ed.* **2009**, *48*, 2474−2499.
(5) Vougioukalakis, G. C.; Philippopoulos, A. I.; Stergiopoulos, T.; Falaras, P. Contributions to the development of ruthenium-based sensitizers for dye-sensitized solar cells. *Coord. Chem. Rev.* **2011**, *255*, 2602−2621.
(6) Clifford, J. N.; Martínez-Ferrero, E.; Viterisi, A.; Palomares, E. Sensitizer molecular structure-device efficiency relationship in dye sensitized solar cells. *Chem. Soc. Rev.* **2011**, *40*, 1635−1646.
(7) Griffith, M. J.; Sunahara, K.; Wagner, P.; Wagner, K.; Wallace, G. G.; Officer, D. L.; Furube, A.; Katoh, R.; Mori, S.; Mozer, A. J. Porphyrins for dye-sensitized solar cells: new insights into efficiency-determining electron transfer steps. *Chem. Commun.* **2012**, *48*, 4145−4162.
(8) Li, C.; Wonneberger, H. Perylene imides for organic photovoltaics: yesterday, today, and tomorrow. *Adv. Mater.* **2012**, *24*, 613−636.
(9) Yen, Y.-S.; Chou, H.-H.; Chen, Y.-C.; Hsu, C.-Y.; Lin, J. T. Recent developments in molecule-based organic materials for dye-sensitized solar cells. *J. Mater. Chem.* **2012**, *22*, 8734−8747.
(10) Li, L.-L.; Diau, E. W.-G. Porphyrin-sensitized solar cells. *Chem. Soc. Rev.* **2013**, *42*, 291−304.
(11) Liang, M.; Chen, J. Arylamine organic dyes for dye-sensitized solar cells. *Chem. Soc. Rev.* **2013**, *42*, 3453−3488.
(12) Zhang, S.; Yang, X.; Numata, Y.; Han, L. Highly efficient dye-sensitized solar cells: progress and future challenges. *Energy Environ. Sci.* **2013**, *6*, 1443−1464.
(13) Wu, Y.; Zhu, W. Organic sensitizers from D-π-A to D-A-π-A: effect of the internal electron-withdrawing units on molecular absorption, energy levels and photovoltaic performances. *Chem. Soc. Rev.* **2013**, *42*, 2039−2058.
(14) Ozawa, H.; Okuyama, Y.; Arakawa, H. Dependence of the efficiency improvement of black-dye-based dye-sensitized solar cells on alkyl chain length of quaternary ammonium cations in electrolyte solutions. *ChemPhysChem* **2014**, *15*, 1201−1206.
(15) Han, L.; Islam, A.; Chen, H.; Malapaka, C.; Chiranjeevi, B.; Zhang, S.; Yang, X.; Yanagida, M. High-efficiency dye-sensitized solar cell with a novel co-adsorbent. *Energy Environ. Sci.* **2012**, *5*, 6057−6060.
(16) Yella, A.; Lee, H.-W.; Tsao, H. N.; Yi, C.; Chandiran, A. K.; Nazeeruddin, M. K.; Diau, E. W.-G.; Yeh, C.-Y.; Zakeeruddin, S. M.; Grätzel, M. Porphyrin-sensitized solar cells with cobalt(II/III)-based redox electrolyte exceed 12% efficiency. *Science* **2011**, *334*, 629−634.
(17) Yella, A.; Mai, C.-L.; Zakeeruddin, S. M.; Chang, S.-N.; Hsieh, C.-H.; Yeh, C.-Y.; Grätzel, M. Molecular engineering of push−pull porphyrin dyes for highly efficient dye-sensitized solar cells: the role of benzene spacers. *Angew. Chem., Int. Ed.* **2014**, *53*, 2973−2977.

(18) Mathew, S.; Yella, A.; Gao, P.; Humphry-Baker, R.; Curchod, B. F. E.; Ashari-Astani, N.; Tavernelli, I.; Rothlisberger, U.; Nazeeruddin, M. K.; Grätzel, M. Dye-sensitized solar cells with 13% efficiency achieved through the molecular engineering of porphyrin sensitizers. *Nat. Chem.* **2014**, *6*, 242−247.
(19) Würther, F. Perylene bisimide dyes as versatile building blocks for functional supramolecular architectures. *Chem. Commun.* **2004**, 1564−1579.
(20) Herbst, W.; Hunger, K. *Industrial Organic Pigments*, 3rd ed.; Wiley: Weinhein, 2006.
(21) Ferrere, S.; Gregg, B. A. New perylenes for dye sensitization of TiO_2. *New J. Chem.* **2002**, *26*, 1155−1160.
(22) Shibano, Y.; Umeyama, T.; Matano, Y.; Imahori, H. Electron-donating perylene tetracarboxylic acids for dye-sensitized solar cells. *Org. Lett.* **2007**, *9*, 1971−1974.
(23) Zafer, C.; Kus, M.; Turkmen, G.; Dincalp, H.; Demic, S.; Kuban, B.; Teoman, Y.; Icli, S. New perylene derivative dyes for dye-sensitized solar cells. *Sol. Energy Mater. Sol. Cells* **2007**, *91*, 427−431.
(24) Edvinsson, T.; Li, C.; Pschirer, N.; Schöneboom, J.; Eickemeyer, F.; Sens, R.; Boschloo, G.; Herrmann, A.; Müllen, K.; Hagfeldt, A. Intramolecular charge-transfer tuning of perylenes: spectroscopic features and performance in dye-sensitized solar cells. *J. Phys. Chem. C* **2007**, *111*, 15137−15140.
(25) Li, C.; Yum, J.-H.; Moon, S.-J.; Herrmann, A.; Eickemeyer, F.; Pschirer, N. G.; Erk, P.; Schöneboom, J.; Müllen, K.; Grätzel, M.; Nazeeruddin, M. K. An improved perylene sensitizer for solar cell applications. *ChemSucChem* **2008**, *1*, 615−618.
(26) Cappel, U. B.; Karlsson, M. H.; Pschirer, N. G.; Eickemeyer, F.; Schöneboom, J.; Erk, P.; Boschloo, G.; Hagfeldt, A. A broadly absorbing perylene dye for solid-state dye-sensitized solar cells. *J. Phys. Chem. C* **2009**, *113*, 14595−14597.
(27) Mathew, S.; Imahori, H. Tunable, strongly-donating perylene photosensitizers for dye-sensitized solar cells. *J. Mater. Chem.* **2011**, *21*, 7166−7174.
(28) Luo, J.; Xu, M.; Li, R.; Huang, K.-W.; Jiang, C.; Qi, Q.; Zeng, W.; Zhang, J.; Chi, C.; Wang, P.; Wu, J. *N*-Annulated perylene as an efficient electron donor for porphyrin-based dyes: enhanced light-harvesting ability and high-efficiency Co(II/III)-based dye-sensitized solar cells. *J. Am. Chem. Soc.* **2014**, *136*, 265−272.
(29) Ferrere, S.; Zaban, A.; Gregg, B. A. Dye sensitization of nanocrystalline tin oxide by perylene derivatives. *J. Phys. Chem. B* **1997**, *101*, 4490−4493.
(30) Yao, Z.; Yan, C.; Zhang, M.; Li, R.; Cai, Y.; Wang, P. *N*-Annulated perylene as a coplanar π-linker alternative to benzene as a low energy-gap, metal-free dye in sensitized solar cells. *Adv. Energy Mater.* **2014**, *4*, doi: 10.1002/aenm.201400244.
(31) Zhang, M.; Wang, Y.; Xu, M.; Ma, W.; Li, R.; Wang, P. Design of high-efficiency organic dyes for titania solar cells based on the chromophoric core of cyclopentadithiophene-benzothiadiazole. *Energy Environ. Sci.* **2013**, *6*, 2944−2949.
(32) Srinivas, K.; Yesudas, K.; Bhanuprakash, K.; Rao, V. J.; Giribabu, L. A combined experimental and computational investigation of anthracene based sensitizers for DSSC: comparison of cyanoacrylic and malonic acid electron withdrawing groups binding onto the TiO_2 anatase (101) surface. *J. Phys. Chem. C* **2009**, *113*, 20117−20126.
(33) Ardo, S.; Meyer, G. J. Photodriven heterogeneous charge transfer with transition-metal compounds anchored to TiO_2 semiconductor surfaces. *Chem. Soc. Rev.* **2009**, *38*, 115−164.
(34) Listorti, A.; O'Regan, B.; Durrant, J. R. Electron transfer dynamics in dye-sensitized solar cells. *Chem. Mater.* **2011**, *23*, 3381−3399.
(35) Yao, Z.; Yang, L.; Cai, Y.; Yan, C.; Zhang, M.; Cai, N.; Dong, X.; Wang, P. Rigidifying the π-linker to enhance light absorption of organic dye-sensitized solar cells and influences on charge transfer dynamics. *J. Phys. Chem. C* **2014**, *118*, 2977−2986.
(36) van Stokkum, I. H. M.; Larsen, D. S.; van Grondelle, R. Global and target analysis of time-resolved spectra. *Biochim. Biophys. Acta* **2004**, *1657*, 82−104.
(37) Berera, R.; Herrero, C.; van Stokkum, I. H. M.; Vengris, M.; Kodis, G.; Palacios, R. E.; van Amerongen, H.; van Grondelle, R.; Gust, D.; Moore, T. A.; Moore, A. L.; Kennis, J. T. M. A Simple artificial light-harvesting dyad as a model for excess energy dissipation in oxygenic photosynthesis. *Proc. Natl. Acad. Sci. U.S.A.* **2006**, *103*, 5343−5348.
(38) Ruban, A. V.; Berera, R.; Ilioaia, C.; van Stokkum, I. H. M.; Kennis, J. T. M.; Pascal, A. A.; van Amerongen, H.; Robert, B.; Horton, P.; van Grondelle, R. Identification of a mechanism of photoprotective energy dissipation in higher plants. *Nature* **2007**, *450*, 575−578.
(39) Ronca, E.; Marotta, G.; Pastore, M.; De Angelis, F. Effect of sensitizer structure and TiO_2 protonation on charge generation in dye-sensitized solar cells. *J. Phys. Chem. C* **2014**, DOI: 10.1021/jp5004853.
(40) Siebrand, W. Radiationless transitions in polyatomic molecules. I. calculation of franck-condon factors. *J. Chem. Phys.* **1967**, *46*, 440−447.
(41) Bisquert, J. Chemical capacitance of nanostructured semiconductors: its origin and significance for nanocomposite solar cells. *Phys. Chem. Chem. Phys.* **2003**, *5*, 5360−5364.
(42) O'Regan, B. C.; Durrant, J. R. Kinetic and energetic paradigms for dye-sensitized solar cells: moving from the ideal to the real. *Acc. Chem. Res.* **2009**, *42*, 1799−1808.
(43) Duffy, N. W.; Peter, L. M.; Rajapakse, R. M. G.; Wijayant, K. G. U. A novel charge extraction method for the study of electron transport and interfacial transfer in dye sensitised nanocrystalline solar cells. *Electrochem. Commun.* **2000**, *2*, 658−662.
(44) O'Regan, B. C.; Bakker, K.; Kroeze, J.; Smit, H.; Sommeling, P.; Durrant, J. R. Measuring charge transport from transient photovoltage rise times. a new tool to investigate electron transport in nanoparticle films. *J. Phys. Chem. B* **2006**, *110*, 17155−17160.
(45) Schlichthörl, G.; Huang, S. Y.; Sprague, J.; Frank, A. J. Band edge movement and recombination kinetics in dye-sensitized nanocrystalline TiO_2 solar cells: a study by intensity modulated photovoltage spectroscopy. *J. Phys. Chem. B* **1997**, *101*, 8141−8155.
(46) Becke, A. D. A New Mixing of Hartree-Fock and local density-functional theories. *J. Chem. Phys.* **1993**, *98*, 1372−1377.
(47) Lynch, B. J.; Fast, P. L.; Harris, M.; Truhlar, D. G. Adiabatic connection for kinetics. *J. Phys. Chem. A* **2000**, *104*, 4811−4815.
(48) Pastore, M.; Mosconi, E.; De Angelis, F.; Gätzel, M. A computational investigation of organic dyes for dye-sensitized solar cells: benchmark, strategies, and open issues. *J. Phys. Chem. C* **2010**, *114*, 7205−7212.
(49) Cossi, M.; Rega, N.; Scalmani, G.; Barone, V. Energies, structures, and electronic properties of molecules in solution with the C-PCM solvation model. *J. Comput. Chem.* **2003**, *24*, 669−681.
(50) Wang, P.; Zakeeruddin, S. M.; Comte, P.; Charvet, R.; Humphry-Baker, R.; Grätzel, M. Enhance the performance of dye-sensitized solar cells by co-grafting amphiphilic sensitizer and hexadecylmalonic acid on TiO_2 nanocrystals. *J. Phys. Chem. B* **2003**, *107*, 14336−14341.
(51) Liu, J.; Li, R.; Si, X.; Zhou, D.; Shi, Y.; Wang, Y.; Wang, P. Oligothiophene dye-sensitized solar cells. *Energy Environ. Sci.* **2010**, *3*, 1924−1928.
(52) Cai, N.; Wang, Y.; Xu, M.; Fan, Y.; Li, R.; Zhang, M.; Wang, P. Engineering of push-pull thiophene dyes to enhance light absorption and modulate charge recombination in mesoscopic solar cells. *Adv. Funct. Mater.* **2013**, *23*, 1846−1854.
(53) Snellenburg, J. J.; Laptenok, S. P.; Seger, R.; Mullen, K. M.; van Stokkum, I. H. M. Glotaran: A Java-based graphical user interface for the r package TIMP. *J. Stat. Softw.* **2012**, *49*, 1−22.